Biodegradable Fibers of Poly(3-hydroxybutyrate) Produced by High-Speed Melt Spinning and Spin Drawing

G. SCHMACK, D. JEHNICHEN, R. VOGEL, B. TÄNDLER

Institute of Polymer Research Dresden, Hohe Strasse 6, 01069 Dresden, Germany

Received 17 August 1999; revised 10 August 2000; accepted 11 August 2000

ABSTRACT: The effects of high-speed melt spinning and spin drawing on the structure and resulting properties of bacterial generated poly(3-hydroxybutyrate) (PHB) fibers were investigated. The fibers were characterized by their degree of crystallinity by differential scanning calorimetry (DSC) and wide-angle X-ray scattering (WAXS), their orientation by WAXS, and the textile physical properties. The WAXS studies revealed that the fibers spun at high speeds and high draw ratios possessed orthorhombic (α modification) and hexagonal (β modification) crystals, the latter as a result of stress-induced crystallization. The fiber structures formed during these processes were fibril-like as the atomic force microscopy images demonstrated. The maximum physical break stress, the modulus, and the elongation at break observed in the fibril-like spin drawn fibers were about 330 MPa, 7.7 GPa, and 37%, respectively. The fibers obtained by a low draw ratio of 4.0 had spherulitic structures and poor textile physical properties. The PHB pellets were analyzed by their degradation during the processes of drying and spinning and by their thermal and rheological properties. © 2000 John Wiley & Sons, Inc. J Polym Sci B: Polym Phys 38: 2841–2850, 2000

Keywords: biodegradable fibers; high-speed melt spinning process; poly(3-hydroxybutyrate); spin-drawing process; wide-angle X-ray scattering; differential scanning calorimetry; atomic force microscopy

INTRODUCTION

Biodegradable polymers represent a relatively new class of materials that have recently gained more and more importance. One of the interesting biodegradable polymers is poly(3-hydroxybutyrate) (PHB), an aliphatic polyester that can be produced by many types of microorganisms in order to store carbon as an intracellular energy source. Because of their bacterial origin, PHBs can be obtained in exceptionally pure form without any inclusion of catalyst residues and as a stereoregular optical active isotactic polyester. Because of this fact, PHB was used in the past as a model polymer for studies of morphology and crystallization kinetics.[1] Many studies reported on the identification of the crystal structure,[2] crystallization,[3] thermal behavior,[3] and chemical composition.[4] On the other hand, there are a number of studies related to the effects of thermoplastic processing conditions on the development of structure and on the resulting mechanical properties of PHB products.[5–9] Numerous thermoplastic processing techniques (e.g., extrusion, injection molding, melt spinning, blowing film) were applied to PHB. Up to now these applications were also limited by high production costs. Nevertheless, PHB is of great interest because of its biotechnological generation, its thermoplastic processability, its unique combination of biodegradability and hydrophobicity, and its medical applications due to its biocompatibility.

Correspondence to: Dr. G. Schmack (E-mail: schmack@ipfdd.de)

Journal of Polymer Science: Part B: Polymer Physics, Vol. 38, 2841–2850 (2000)

In the present study we were primarily concerned with the effect of the melt spinning conditions, high-speed melt spinning, and spin-drawing process on the development of the structural hierarchy in the fibers and the relation to the textile physical properties. An investigation was carried out on the effects of spinning conditions on the orientation in the crystalline regions and especially the development of a strain-induced crystalline structure (β modification).

EXPERIMENTAL

Materials

The virgin material of the bacterial generated polyester PHB was only available in powder form. The powder was vacuum dried at 60 °C at least 48 h to remove moisture. In preparation for the spinning experiments, the dried powder was pelletized in a twin-screw extruder. Prior to melt spinning the pellets were dried again in a drum dryer at a temperature of 120 °C under a vacuum for 16 h and afterward filled and kept under a nitrogen atmosphere. The water content of the pellets was determined by coulombmetric titration at 120 °C according to Karl Fischer. The samples were heated in an oven and the water was transported to the titration vessel. The water content of the dried pellets was 0.01%.

The PHB was characterized with regard to its degradation during the processes of pelletization and spinning. For that aim the thermal and rheological properties were measured.

Viscosity of Solutions

The PHB samples were dissolved in chloroform and an appropriate concentration series was produced. The relative viscosities of the solutions were measured at 20 °C in an Ubbelohde capillary viscosimeter.

Dynamic Rheological Measurements

The oscillating measurements with PHB melts were carried out with samples of the virgin powder, pellets, and as-spun fibers by means of a rotational rheometer (ARES, Rheometric Scientific, Inc.). The geometry chosen for these measurements was a plate/plate arrangement (25-mm plate diameter, 2-mm gap width). The measurements were carried out under a nitrogen atmosphere at 200 °C in a shear frequency range of 10^{-1}–10^{+2} rad/s. In addition, a temperature sweep was recorded beginning at 190 and 200 °C at a mean shear frequency of 1 rad/s and a cooling rate of 5 K/min. The complex melt viscosity (η^*) was determined.

Spinning Experiments

High-Speed Spinning

The fibers were spun using a spinning device at the Institute of Polymer Research (Dresden) as described elsewhere.[10] The equipment consisted of an extruder (18-mm screw diameter) with a spinning pump, a spin pack, heated godets, and two winders for take-up velocities up to 2000 m/min and a range of 2000–6000 m/min, respectively. During the melt spinning the hopper system was maintained in an inert atmosphere in order to minimize the hydrolytic degradation and/or the oxidation. To investigate the influence of the spinning speed on the properties of the filaments, the mass throughput of the spinning pump was kept constant at 16.2 g/min to reach a homogeneous melt treatment up to the spinneret, independent of the spinning speed. The geometry of the extruder screw was chosen in the usual way for polyester, and the conditions of extrusion were adapted according to the range of the melting temperature of PHB. Temperatures of 165, 175, 180, 173, and 173 °C were used. The spinning pressure was about 80 bar. The spin pack contained two double filter screens. A 12-hole spinneret was used, and yarns with 12 filaments were spun. The diameter of a single spinneret hole was 0.3 mm and its length was 0.6 mm. The temperature of the first godets was 80 °C. The filaments were moistened with a nonaqueous preparation (Silastol). The filaments were taken up by means of a winder in a range of 2000–3500 m/min.

Spin Drawing

The spin drawing was carried out using the same equipment. The filaments were taken up at about 250 m/min and were drawn between the first and the second heated godets. The temperatures of the godets were chosen in a way that the temperatures of the first godets were at 40 and 45 °C and the temperatures of the second godets were at 50 and 60 °C. The draw ratios (DR) were varied from 4.0 to 6.9, which means that the velocities of the second godets were between 800 and 1380 m/min.

Characterization of Fibers

Stress–strain curves, differential scanning calorimetry (DSC) scans, and wide-angle X-ray scattering (WAXS) scans were determined. The sound velocity was measured for the fibers produced using the different technologies to show the correlation between the textile physical values, the degree of crystallization, and the orientation of the fibers. Typical 3-dimensional (3-D) surface topographic images of the fibers were made by means of an atomic force microscopy (AFM).

Stress–Strain Measurements

The mechanical properties were measured by means of a Z 010 testing machine (Fa. Zwick GmbH and Co., Ulm, Germany) according to DIN 53834. The average of the tensile test results on 10 specimens of each run were reported. The physical break stress and the elongation at break were calculated.

Sound Velocity Measurements

An SLM-1 measurement system (Ilse Elektrotechnik, Guben, Germany) was applied to determine the sound velocity (v_v) of a pulse wave front running through the yarn. The measuring frequency was 10 MHz. The measuring distance on the filament was 30 cm. The sonic modulus was calculated.

Thermal Analysis by DSC

The DSC measurements were carried out on the virgin powder, the pellets, and the fibers in the temperature range of 40–200 °C with a heating rate of 20 K/min under nitrogen flow. The crystalline content of the specimens was determined by rating the difference between the enthalpies of melting and crystallization peak areas and the reference melting enthalpy of the 100% crystalline polymer (146 J/g).[7]

WAXS Investigations

The WAXS patterns were obtained in transmission by means of Cu-Kα radiation using a four-circle P4 diffractometer (Siemens AG, Karlsruhe) equipped with a HiStar/GADDS area detector system (Siemens Analytical X-Ray Instruments Inc., Madison, WI). The equatorial and meridional scattering range included $2\theta \approx 5$–$40°$. For the meridian scattering the fibers were tilted about 15°, corresponding to the scattering angle of the $\alpha(002)$ reflection.

Table I. Comparison of Intrinsic Viscosities (η_{int}) and Viscosity-Average Molecular Weights (M_v) of PHB Samples

Samples	η_{int} (dL/g)	M_v (g/mol)
Virgin powder	3.48	540,000
Pellets	2.54	360,000
As-spun fibers	1.45	175,000

AFM

The topography of the fibers was measured with a Nanoscope III AF microscope (Digital Instrument Inc., Santa Barbara, CA). A cantilever with an integrated tip was used as the microscopic force sensor. The fiber was brought into continuous contact with the Si tip of the cantilever and raster scanned. Topographical 3-D maps of the surface were constructed by plotting the local sample height versus the horizontal probe tip position. The conditions were 1.5 V (constant force mode), a scan width of 5 μm (x–y scan range), a z scan of 500 nm, and a scan rate of 5 Hz. The measurements were done in air in contact mode. The images were treated with the flatten procedure.

RESULTS AND DISCUSSION

Viscosity Solutions

The intrinsic viscosities (η_{int}) for the virgin powder, the pellets, and the as-spun fibers were calculated from the relative viscosities according to an empirical Huggins relationship. The viscosity-average molecular weight (M_v) was estimated by means of the relationship[11] $\eta_{int} = 1.18 \times 10^{-4} \times M_v^{0.78}$. A comparison of the estimated molecular weights of the samples (Table I) shows that considerable thermal degradation takes place during the pelletization and during the spinning process afterward.

Lemoigne[12] had already regarded PHB as melt unstable in 1925. The degradation mechanism by the β elimination to crotonic acid at temperatures slightly above its melting point was described by Macrae and Wilkinson.[13] Holmes[7] showed results of a series of melt flow index tests on PHB with a weight-average molecular weight (M_w = 500,000

g/mol) over a range of processing temperatures and suggested minimizing the melt temperatures and residence times to provide the degradation within defensible limits.

Dynamic Rheological Measurements

Figure 1 shows the dependence of the melt viscosity (η^*) of the virgin powder, the pellets, and the as-spun fibers measured at 200 °C as a function of the frequency. The measurements were carried out from the higher to the lower shear frequencies to observe the thermal degradation occurring during the measured time, because by measuring in the other direction, the degradation of the polymers resulting in a viscosity decrease would be overlapped by the decrease of the complex viscosity function as a result of the structure-viscous behavior. The decrease of the melt viscosity at lower shear frequencies indicated substantial degradation during the rheological measurement. It is obvious from this that the thermal degradation is enhanced at a residence time above 5 min, corresponding to a frequency range of <10 rad/s. The differences between the functions of the complex η^* of the virgin powder, the pellets, and the as-spun fibers clearly show the thermal degradation as originating from the existing thermal processing, the pelletization, and the melt spinning afterwards. As a result of the thermal degradation, a molecular weight of 175,000 g/mol was

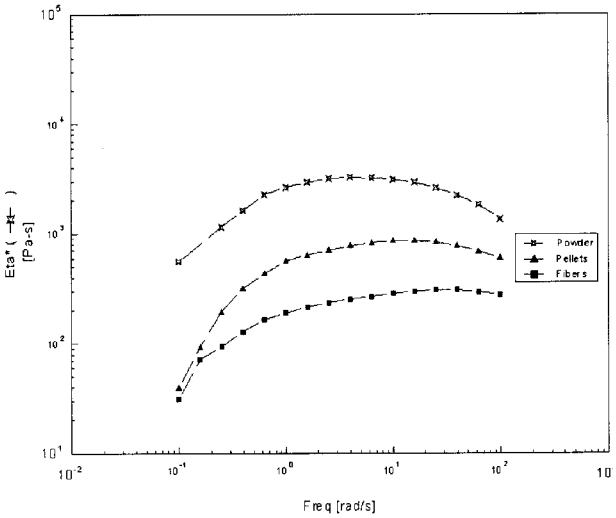

Figure 1. Melt viscosities of the virgin powder, pellets, and as-spun fibers measured at 200 °C as a function of the frequency.

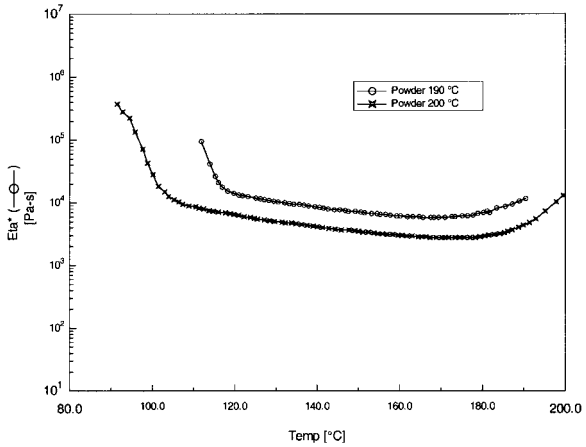

Figure 2. The melt viscosity of the virgin powder measured at starting temperatures of 190 and 200 °C as a function of the temperature.

obtained that preserved the spinability of the PHB.

The influence of different starting temperatures on the thermal degradation of the PHB powder is shown in Figure 2. The measurements were started at 190 and 200 °C. The temperature sweeps show the overlay of the influence of the decreasing measurement temperature and the thermal degradation and the beginning of the crystallization on the course of the viscosity function. The influence of the different starting temperatures on the course of the viscosity functions is especially clear. The higher the starting temperature, the stronger the thermal degradation at the beginning of the measurement. In the range below 160 °C up to the crystallization temperature, the viscosity functions of the samples follow the usual temperature dependence of the melt viscosity. The flow activation energies of the samples are about 26 kJ/mol. The beginning of the crystallization depends on the starting temperature of the measurements. A starting temperature of 200 °C shifts the beginning of the crystallization about 20 K to lower temperatures with a starting temperature of 190 °C. This can be explained as self-seeding by nucleation by unmelted PHB crystals at 190 °C, because the temperature of the melt does not exceed the melting range by more than a few degrees in order to melt all the PHB nuclei (Fig. 3).

Thermal Analysis

Figure 3 shows DSC scans of the virgin powder and the undried and dried pellets. The scans il-

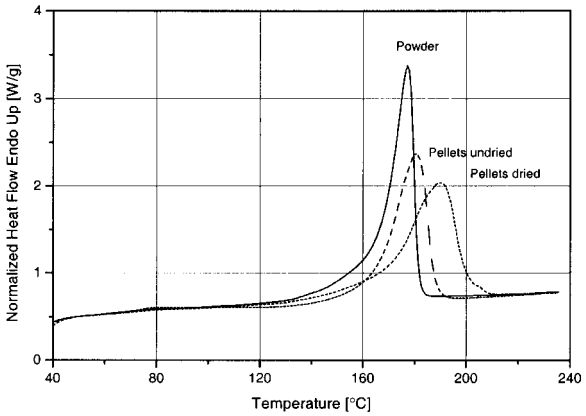

Figure 3. DSC scans of the virgin powder and the undried and dried pellets.

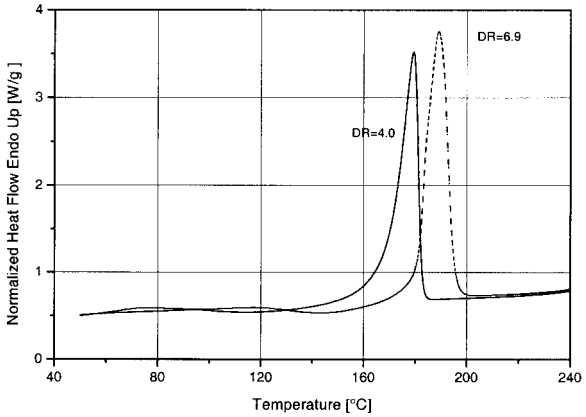

Figure 4. DSC scans of fibers drawn at ratios of 4.0 and 6.9.

lustrate the shift of the melting temperature maximum (T_{max}), the changes of the distribution of the crystallite sizes, and the degree of crystallinity (α) as effects of the processing, the pelletization, and the drying (Table II). The shift of the melting temperatures to higher values has great influence on the choice of the temperature profile of the spinning extruder and, consequently, on the degree of degradation during the spinning process.

Figure 4 demonstrates the effect of the spin-drawing conditions on the DSC scans and consequently on the fiber structure. In comparison with the DSC scans of the pellets and the powder, the drawn fiber ones illustrate a narrow distribution of crystallite sizes. Table III shows the different influences of the draw ratios and the temperatures of the first (40–50 °C) and second godets (45–60 °C) on the melting temperature maxima.

In absence of the molecular orientation the crystallization velocity of PHB is so slow that the PHB is easily quenched to a noncrystalline, amorphous state. The crystallization will be developed only in the postcrystallization process during the conditioning. This appears to be the case in the filaments spun at a low draw ratio of 4.0. With increasing spinning speeds and with increasing draw ratios a molecular orientation is developed in the spinline and the crystallization velocity increases. The increase in crystallization velocity is sufficient to compensate the increased cooling rate in the spinning process. The effect is that the PHB is able to crystallize at a definite spinning velocity and draw ratio as a result of stress-induced nucleation, as the relatively highly oriented crystalline fraction shows.

The crystalline content of the spin-drawn fibers appeared to be dependent on the 40–50 and 45–60 °C temperatures of the godets with values of 48 and 55%, respectively.

In the investigated range of the spinning speed (2000–3500 m/min) an influence on the melting temperature and on the degree of crystallinity of the high speed spun fibers could not be observed. The melting temperature maxima was about 189 °C, and the crystalline content was about 48%.

Table II. Melting Temperature Maxima (T_{max}) and Degree of Crystallinity (α) of PHB Materials

Material	T_{max} (°C)	α (%)
Virgin powder	177.2	72
Undried pellets	180.6	53
Dried pellets	189.9	69

The materials are those in Figure 3.

Stress–Strain Measurements

Figure 5 shows the stress–strain curves of the spin drawn fibers dependent on the draw ratio

Table III. Melting Temperature Maxima (T_{max}) of Spin-Drawn Fibers Dependent on Draw Ratio (DR) and Temperatures (T) of First and Second Godets

T = 40–50 °C		T = 45–60 °C	
DR	T_{max} (°C)	DR	T_{max} (°C)
4.0	179.2	5.4	185.3
4.5	181.6	5.9	185.6
5.0	184.8	6.4	186.2
5.5	187.7	6.9	188.9

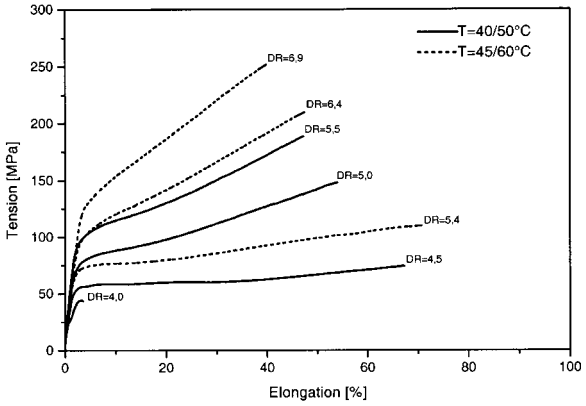

Figure 5. Stress–strain curves of the fibers dependent on the draw ratio and the different temperatures of the first (40 and 45 °C) and second godets (50 and 60 °C).

(4.0–6.9) and on the different temperatures of the first and second godets (40–50 and 45–60 °C, respectively). The draw ratio is known to be determined by the degree of chain extension and the molecular orientation relative to the fiber axis. A marked difference exists between the curves of the fibers drawn by a draw ratio of 4.0 and 4.5. The fibers drawn at a draw ratio of 4.0 are brittle and have no significant elongation at break and tensile strength. The draw ratio of 4.5 allows the production of fibers with an acceptable elongation at break. Higher tenacity values were reached in the range of higher temperatures of the first (40–50 °C) and second godets (45–60 °C) and the higher draw ratios.

Figure 6 shows the typical stress–strain curves of drawn fibers (DR = 6.9) conditioned at room

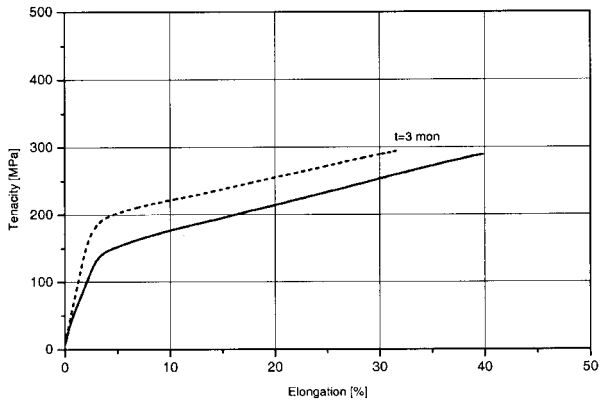

Figure 6. Stress–strain curves of the fibers drawn at a ratio of 6.9 as dependent on the conditioning after 3 days and 3 months.

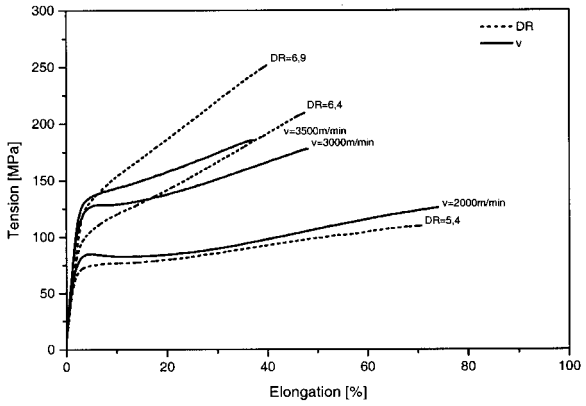

Figure 7. Stress–strain curves of spin drawn fibers in relation to those of the high-speed spun fibers.

temperature for 3 days and 3 months. Neither embrittlement of the fibers nor deterioration of the fiber properties due to the secondary crystallization took place to a large extent.

Figure 7 shows the stress–strain curves of the spin-drawn fibers and the high-speed spun fibers. In Table IV the textile physical values (elongation at break, physical break stress, and sonic modulus) are represented that are dependent on the spinning speed and the draw ratio.

WAXS Measurements

By means of fiber patterns, the crystallinity and the orientation were investigated as dependent

Table IV. Textile Elongation at Break (ε_H), Physical Break Stress (σ), and Sonic Modulus (E) Dependent on Spinning Speed (v) and Draw Ratio (DR) of Temperatures (T) of First and Second Godets

v (m/min)	ε_H (%)	σ (MPa)	E (GPa)
2000	72.2	228	5.8
3000	48.4	281	7.1
3500	35.9	250	7.6
DR			
	T_1/T_2 = 40 and 50 °C		
4.0	10.1	52	—
4.5	60.4	108	—
5.0	52.5	220	—
5.5	59.7	263	5.6
	T_1/T_2 = 45 and 60 °C		
5.4	70.6	178	5.2
6.4	45.3	310	6.8
6.9	37.2	330	7.7

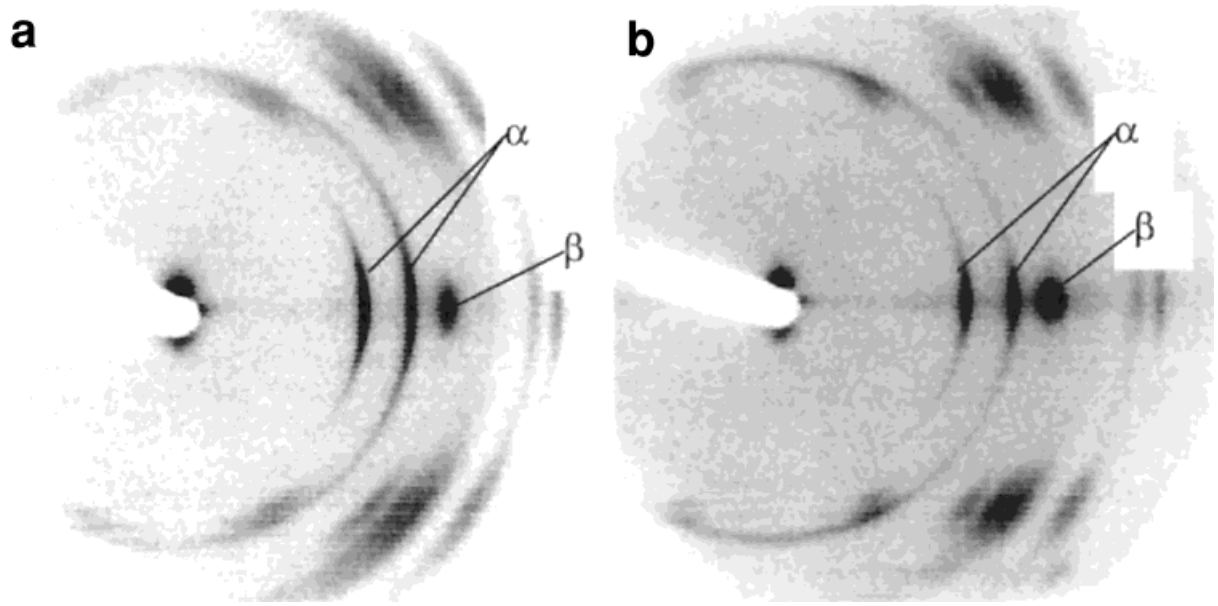

Figure 8. The equatorial X-ray scattering area near the α(020)/(110) and β(100) reflections for fibers spun by v = (a) 2000 and (b) 3500 m/min.

on the spinning and drawing conditions. Typical X-ray diffraction patterns of the equatorial scattering areas for the high-speed spun and the spin-drawn fibers are shown in Figures 8 and 9, respectively. The reflections are indicated using the orthorhombic crystal structure (α modification, 2/1 helix) described by Yamamoto et al.[8] and Kusaka et al.[14] In most samples an additional crystal structure exists that can be assigned to the hexagonal β modification (zigzag conformation) reported by Orts et al.[15] for highly oriented fiber samples.

The appearance of both crystalline modifications in the fibers indicates that PHB chains crys-

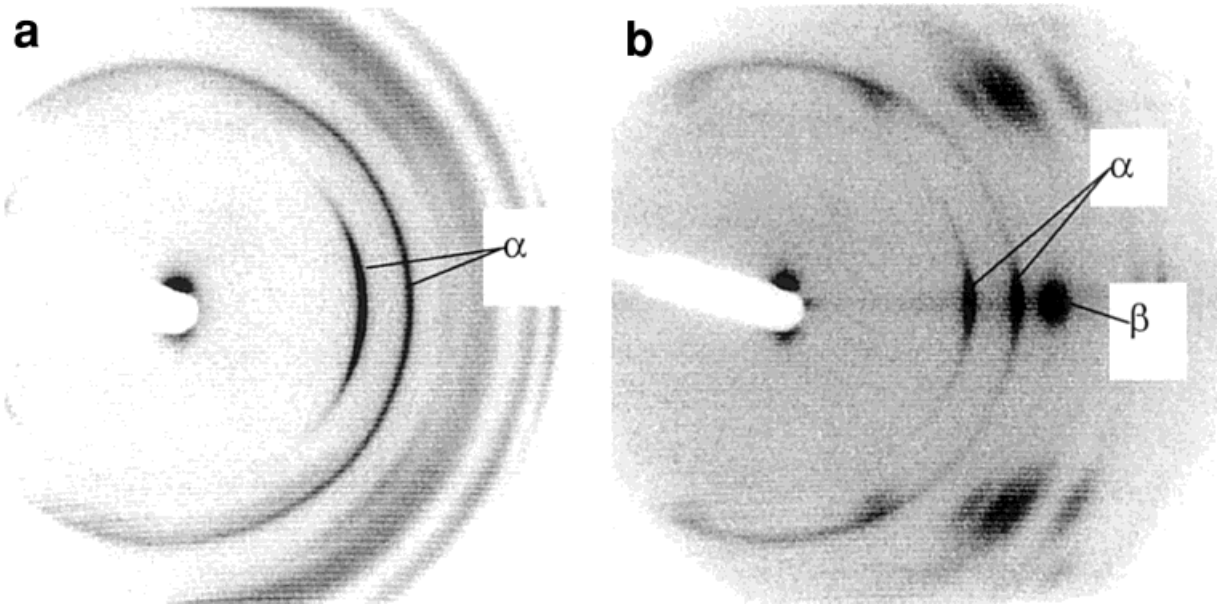

Figure 9. The equatorial X-ray scattering area near the α(020)/(110) and β(100) reflections for fibers spun drawn at DR = (a) 4.0 and (b) 6.9.

tallize in a helical, as well as in a planar, zigzag conformation. Obviously, the stress reached during the process of fiber formation determines the amount of crystalline modifications. This can be demonstrated by the comparison of the spin-drawn fibers. At a draw ratio of 4.0 [Fig. 9(a)], no reflections of the hexagonal modification can be detected (within the error limits). The stress resulting from the spin-drawing process at these conditions seems to not be high enough to start a stress-induced crystallization, which is the case in fibers spun at higher draw ratios [Fig. 9(b)]. The fibers spun in the range of high spinning speeds show very similar WAXS patterns with rather narrow reflections of both crystalline modifications [Fig. 8(a,b)].

Figures 10 and 11 show the order and orientation parameters of the high-speed spun and spin-drawn fibers, respectively. These parameters were determined in a simple manner. The crystallinity was characterized by an equatorial crystallinity index as the sum of all crystalline reflection areas inside the scattering range $2\theta = 9–29°$ in relation to the total scattering intensity (without background) in the same range (only for the equatorial trace). These values were much higher than the crystallinity for the isotropic material (determined in the same way; e.g., WAXS on isotropic foils ≈ 0.65), as well as that found by DSC. The orientation degrees were determined by means of the half path width of the azimuthal intensity distribution of the $\alpha(020)$ and $\beta(100)$ reflections around the equatorial trace. Although the evaluation of the reflections on the meridian should be preferred for the orientation characterization, this approach failed because of the convolution of several reflections.

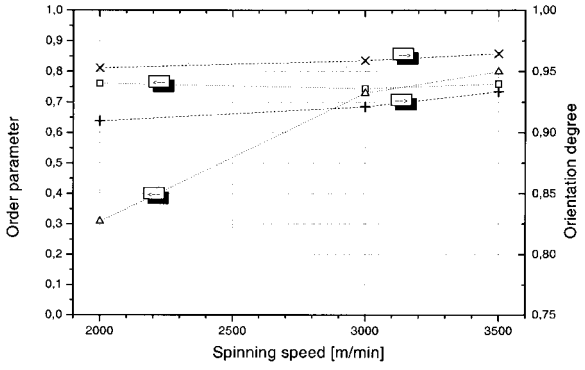

Figure 10. WAXS results dependent on the spinning speed: (·) equatorial crystallinity index, (Δ) $\beta(100)/\alpha(020)$ ratio, (+) orientation degree of $\alpha(020)$, and (×) orientation degree of $\beta(100)$.

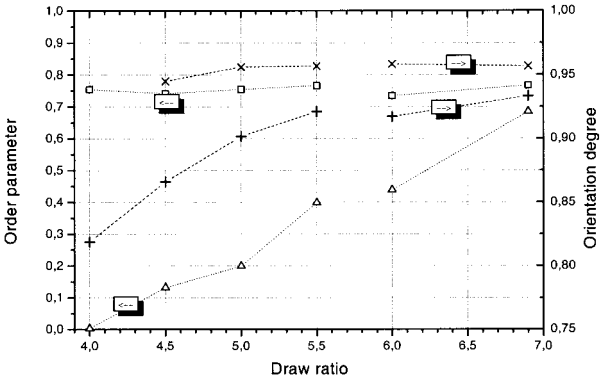

Figure 11. WAXS results dependent on the draw ratio: (·) equatorial crystallinity index, (Δ) $\beta(100)/\alpha(020)$ ratio, (+) orientation degree of $\alpha(020)$, and (×) orientation degree of $\beta(100)$.

The crystallinity index of the high-speed spun fibers was on the order of 0.75 and tended to remain constant with increasing spinning speed. The β/α relations determined as a $\beta(100)/\alpha(020)$ ratio [means: absolute peak height of $\beta(100)$ in relation to the $\alpha(020)$ one obtained on the equatorial trace] increased with the spinning speed approaching a plateau. The orientation degrees increased marginally with the spinning speed when the β value was larger than the α one (Fig. 10).

In the spin-drawn fibers (Fig. 11) the different temperature treatments of the godets (40/50 and 45/60 °C) must be considered. The equatorial crystallinity index of these fibers was quite constant whereas the peak height ratio $\beta(100)/\alpha(020)$ showed a strong ascent dependent on the draw ratio. The increasing orientation was reflected by the increasing values of the β, as well as α, orientation degrees in which the dependence of the α one is stronger.

AFM Images

Figure 12 shows typical 3-D surface topographic images of the fibers drawn by a draw ratio of 4.0 [Fig. 12(a)] and 6.9 [Fig. 12(b)]. The surfaces of the fibers differ considerably. Depending on the draw ratio, spherulitic or fibril-like surface structures were formed. The textile physical properties of the fibers can be explained by these different structures. The fibers spun by a draw ratio of 4.0 are brittle without a sufficient elongation at break visible in the stress–strain curve (Fig. 5). The fibers spun by a draw ratio of 6.9 show completely different stress–strain behavior with a sufficient

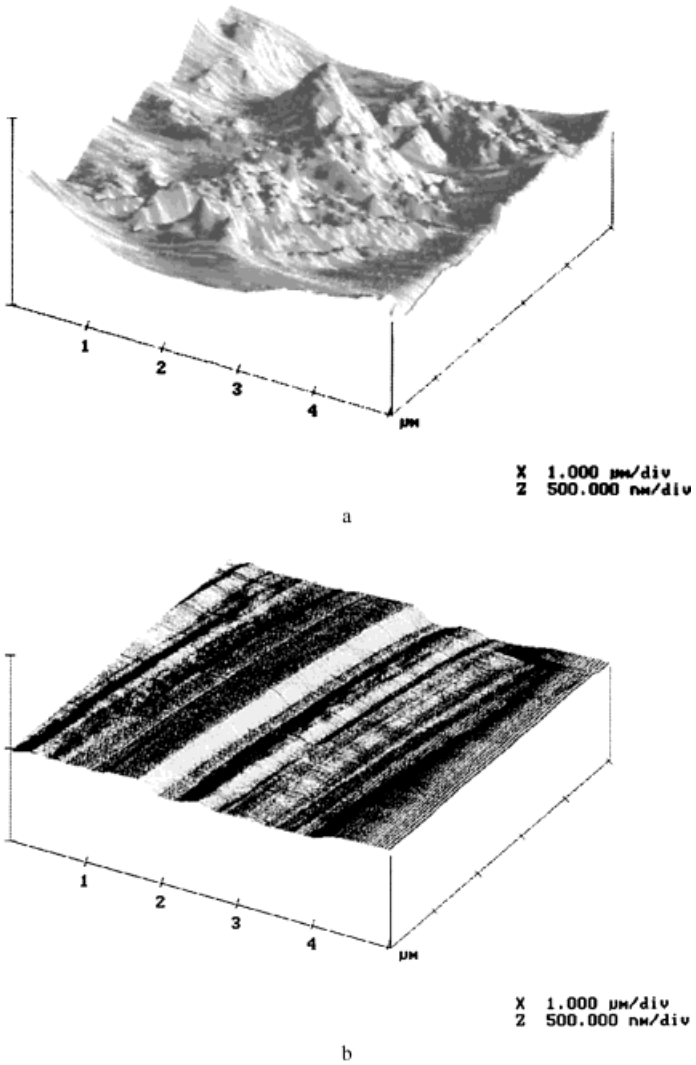

Figure 12. Three Dimensional surface topographic images of fibers drawn at DR = (a) 4.0 and (b) 6.9.

elongation at break and sufficient tenacity, as can be seen from the stress–strain curve (Fig. 5).

CONCLUSIONS

hPHB was spun in a high-speed spinning process with a take-up velocity of 2000–3500 m/min and in a spin-drawing process with draw ratios of 4.0–6.9. A high molecular weight virgin PHB is required in order to get appropriate textile physical values of the tenacity and the elongation at break because of considerable thermal degradation during the pelletization and during the spinning process. A stress-induced crystallization was shown in fibers spun at high speed and in those spun with a high draw ratio. The WAXS results of these fibers indicated two different crystal modifications. The fiber structures formed during these processes were fibril-like as the AFM images demonstrated. The structures could be directly correlated with the increased textile physical properties in comparison to the fibers that were obtained by a low draw ratio of 4.0. These had spherulitic structures and poor textile physical properties. The maximum physical break stress and the modulus observed in the fibril-like spin-drawn fibers were about 330 MPa and 7.7 GPa, respectively, with an elongation at break of 37%.

The authors wish to thank Mr. F. Pursche of the Institute of Polymer Research Dresden for the pelletization of the PHB powder. Furthermore, the authors are grateful to Mr. U. Hänggi from Fa. Biomer for stimulating discussions on thermoplastic processing conditions and on the development of the structure.

REFERENCES AND NOTES

1. Barham, P. J.; Keller, A.; Otun, E. L.; Holmes, P. A. J Mater Sci 1984, 19, 2781–2794.
2. Yokoichi, M.; Chatani, M.; Tadokoro, H.; Teranishi, K.; Tani, H. Polymer 1973, 14, 267–272.
3. Kunioka, M.; Tamaki, A.; Doi, Y. Macromolecules 1989, 22, 694–700.
4. Bloembergen, S.; Holden, D.; Hamer, G. K.; Bluhm, T. L.; Marchessault, R. H. Macromolecules 1986, 19, 2865–2871.
5. Wang, Y. D.; Yamamoto, T.; Camak, M. J Appl Polym Sci 1996, 61, 1957–1970.
6. Furuhasi, Y.; Ito, H.; Kikutani, T.; Yamamoto, T.; Kimizu, M.; Camak, M. J Polym Sci Part B: Polym Phys 1998, 36, 2471–2482.
7. Holmes, P. A. In Developments in Crystalline Polymers—2; Bassett, D. C.; Ed.; Elsevier Applied Science: New York, 1988; pp 1–65.
8. Yamamoto, T.; Kimizu, M.; Kikutani, T.; Furuhashi, Y.; Cakmak, M. Int Polym Process 1997, 12, 29–37.
9. Mitomo, H.; Barham, P. J.; Keller, A. Polym Commun 1988, 29(4), 112–115.
10. Schmack, G.; Beyreuther, R.; Hofmann, H.; Müller, U.; Jehnichen, D. Chem Fibers Int 1995, 45, 475–477.
11. Akita, S.; Einaga, Y.; Miyaki, Y.; Fujita, H. Macromolecules 1976, 9, 774–780.
12. Lemoigne, M. Ann Inst Pasteur 1925, 39, 144–173.
13. Macrae, R. M.; Wilkinson, J. F. J Gen Microbiol 1958, 19, 210–222.
14. Kusaka, S.; Iwata, T.; Doi, Y. Macromol Sci Pure Appl Chem 1998, A35, 319–335.
15. Orts, W. J.; Marchessault, R. H.; Bluhm, T. L.; Hamer, G. K. Macromolecules 1990, 23, 5368–5370.